The Astrophysical Journal, 668:611–624, 2007 October 10

TERMINATION SHOCK ASYMMETRIES AS SEEN BY THE *VOYAGER* SPACECRAFT: THE ROLE OF THE INTERSTELLAR MAGNETIC FIELD AND NEUTRAL HYDROGEN

Nikolai V. Pogorelov,[1] Edward C. Stone,[2] Vladimir Florinski,[1] and Gary P. Zank[1]

Received 2007 April 12; accepted 2007 June 6

ABSTRACT

We show that asymmetries of the termination shock due to the influence of the interstellar magnetic field (ISMF) are considerably smaller in the presence of neutral hydrogen atoms, which tend to symmetrize the heliopause, the termination shock, and the bow shock due to charge exchange with charged particles. This leads to a much stronger restriction on the ISMF direction and its strength. We demonstrate that in the presence of the interplanetary magnetic field the plane defined by the local interstellar medium (LISM) velocity and magnetic field vectors does not exactly coincide with the plane defined by the interstellar neutral helium and hydrogen velocity vectors in the supersonic solar wind region, which limits the accuracy of the inferred direction of the ISMF. We take into account the tilt of the LISM velocity vector with respect to the ecliptic plane and show that magnetic fields as strong as 3 μG or greater may be necessary to account for the observed asymmetry. Estimates are made of the longitudinal streaming anisotropy of energetic charged particles at the termination shock caused by the nonalignment of the interplanetary magnetic field with its surface. By investigating the behavior of interplanetary magnetic field lines that cross the *Voyager 1* trajectory in the inner heliosheath, we estimate the length of the trajectory segment that is directly connected by these lines to the termination shock. A possible effect of the ISMF draping over the heliopause is discussed in connection with radio emission generated in the outer heliosheath.

Subject headings: ISM: kinematics and dynamics — magnetic fields — MHD — shock waves — solar wind

1. INTRODUCTION

The properties of the local interstellar medium (LISM), whose interaction with the solar wind (SW) creates the heliosphere, are incompletely known (Möbius et al. 2004). This is especially true if we consider the strength and direction of the interstellar magnetic field (ISMF). On the other hand, there are strong indications that the ISMF is responsible for several important phenomena that may well be related to *Voyager* observations.

1. According to Zank (1999), Jokipii et al. (2004), and Stone et al. (2005) nonalignment of the interplanetary magnetic field (IMF) with the termination shock (TS) surface can result in longitudinal streaming anisotropies of energetic charged particles observed by *Voyager 1* (V1) at ~85 AU (Krimigis et al. 2003; McDonald et al. 2003) in cases when the ISMF component parallel to the ecliptic plane makes the TS east-to-west asymmetric. This could happen because V1 was connected to an IMF line reentering the supersonic solar wind region after previous penetration into the heliosheath.

2. *Voyager 2* (V2), which is now at ~82 AU from the Sun and traveling in the southern hemisphere at approximately the same angle to the ecliptic plane as V1 did in the northern hemisphere (30.5° vs. ~35°), has already started measuring similar anisotropies. This led Stone et al. (2005) to the conclusion that the termination shock distances to the Sun differ by about 7–10 AU at V1 and V2 heliolatitudes. The ISMF tilt with respect to the LISM velocity is known to produce such asymmetries (see, e.g., Fahr et al. 1988; Pogorelov & Matsuda 1998; Ratkiewicz et al. 1998, 2000; Ratkiewicz & Ben-Jaffel 2002; Pogorelov et al. 2004).

3. Recent measurements from the Solar Wind Anisotropies (SWAN) experiment on board the *Solar and Heliospheric Observatory* (*SOHO*) satellite discovered a divergence of the neutral hydrogen (H) flow of ~4° with respect to the neutral helium (He) direction at distances less than 10 AU to the Sun (Lallement et al. 2005). These two vectors should be parallel in an unperturbed LISM that is homogeneous on scales less than several collisional and charge exchange mean free paths. The flow of helium is not deflected by the heliospheric boundary due to its large mean free path with respect to collisions with plasma particles, whereas the flow of hydrogen is deflected from its original direction ($\boldsymbol{V}_\infty$) due to charge exchange with H^+ in the heliosphere, presumably due to misalignment between the ISMF and LISM velocity vectors by some angle $\alpha_{\rm H}$ (Izmodenov et al. 2005). Pogorelov & Zank (2006) have shown that a deflection of this order can be obtained for different orientations of the ISMF. Moreover, the plane defined by the He and H velocity vectors (the hydrogen deflection plane [HDP]) does not exactly coincide with that determined by the vectors $\boldsymbol{B}_\infty$ and $\boldsymbol{V}_\infty$ (the *B*-*V* plane). This is due to the presence of the IMF, which eliminates the plane symmetry of the heliosphere (Pogorelov et al. 2004). A simple analysis shows that if the angle between the H and He velocity vectors projected on the *B*-*V* plane is $\alpha_\parallel = 4^\circ$, then even a small angle $\alpha_\perp = 1^\circ$ between their projection on the plane orthogonal to the *B*-*V* plane will result in the angle $\alpha_{\rm H} = \arctan(\tan 1^\circ/\tan 4^\circ) \approx 14^\circ$ between the *B*-*V* plane and the local HDP ($\boldsymbol{v}_{\rm H}$-$\boldsymbol{v}_{\rm He}$ plane). Thus, to go beyond the results of Lallement et al. (2005) it is essential to perform observations that distinguish between deflections along different lines of sight. Such observations are expected from the *Interstellar Boundary Explorer* (*IBEX*) mission.

4. Pogorelov et al. (2006) showed that an ISMF with a strength of about 3–5 μG can result in a highly asymmetric distribution of neutral hydrogen throughout the heliosphere. Such distributions are likely to affect Lyα absorption profiles in directions toward different nearby stars (Wood et al. 2004, 2006). As a result, such observations can be used to rule out certain orientations and strengths of the ISMF.

[1] Institute of Geophysics and Planetary Physics, University of California, Riverside, CA 92521; nikolaip@ucr.edu, vflorins@ucr.edu, zank@ucr.edu.
[2] California Institute of Technology, Pasadena, CA 91125; ecs@srl.caltech.edu.

5. The ISMF strength B_∞ and direction can potentially affect the distribution of the 2–3 kHz radio emission sources which are believed to originate ahead of the heliopause (HP) that separates the solar wind from the LISM (Frisch 2003; Kurth & Gurnett 2003). It was suggested that such emission is generated when shocks associated with global merged interaction regions (GMIRs) accelerate electrons in the region ahead of the heliopause, where the electron distribution has a superthermal tail produced by a priming process due to resonant acceleration of lower hybrid waves generated by high-temperature pickup ions (Cairns & Zank 2002). The sources of this radio emission are roughly aligned parallel to the Galactic plane, thus making an angle of about 60° with respect to the solar ecliptic plane. As shown by Cairns et al. (2006) and Mitchell et al. (2007) draping of the magnetic field over the heliopause leads to an approximately linear band aligned with $\boldsymbol{B}_\infty$, where the magnetic field is large near the heliopause and where the necessary conditions for the generation of the emission are satisfied. An alternative idea, suggested by Gurnett et al. (2006), is that the source band corresponds to the heliopause region where $\boldsymbol{B}_\infty \perp \boldsymbol{n}$ for a GMIR shock normal $\boldsymbol{n}$, which may result in the radio source location in the plane being close to the Galactic plane. As noted by Cairns et al. (2006) this idea is not incompatible with the draping/GMIR theory, and the combination of both should be explored more carefully.

6. Heerikhuisen et al. (2006b, 2007), on the basis of an MHD-kinetic simulation, have recently shown that all ISMF-induced asymmetries are readily seen in the energetic neutral atom (ENA) all-sky maps. Comparing these maps with those to be provided by the *IBEX* spacecraft after launch (McComas et al. 2004, 2006) should help us determine the properties of the LISM.

In this paper, we emphasize the crucial importance of neutral hydrogen atoms for possible asymmetries of the termination shock and heliopause and show that these asymmetries are significantly overestimated by purely MHD models (Pogorelov & Matsuda 1998; Ratkiewicz et al. 1998; Pogorelov et al. 2004; Opher et al. 2006). We also deduce some restrictions on $\boldsymbol{B}_\infty$, which are necessary to allow for the observed asymmetries. The paper is structured as follows. In § 2 we examine the TS asymmetry in the V1 and V2 directions for different orientations of $\boldsymbol{B}_\infty$. Section 3 deals with the magnetic-field-induced east-west asymmetries of the TS and its crossings by the IMF field lines multiple times. We use the nonlinear guiding center (NLGC) theory to determine the dependence of the longitudinal streaming anisotropy of 1 MeV protons on the angle between the IMF and the TS normal. This is further used to relate the observations to the theory. According to the scenario suggested by McComas & Schwadron (2006) plasma particles are possibly more easily injected into the shock-acceleration process at the TS flanks and, because of the IMF lines crossing the TS there, have longer time in contact with the shock. As a result, these lines are deeper in the heliosheath, so the spacecraft should see steadily rising fluxes of higher energy particles and the unrolling of the anomalous cosmic ray (ACR) spectrum. We utilize three-dimensional geometrical estimations of the distance V1 can travel in the inner heliosheath while being *directly connected* to the TS by one of the IMF lines (after that they connect only after spiraling one or more times completely around the TS). Section 3 addresses the appearance of bandlike structures in the magnetic field distribution in the outer heliosheath and its possible effect on the distribution of 2–3 kHz radio emission sources. Finally, we draw some quantitative conclusions about the ISMF strength and direction that will make the TS sufficiently asymmetric to meet certain observation-based hypotheses.

2. TERMINATION SHOCK ASYMMETRY IN THE *VOYAGER 1* AND *VOYAGER 2* DIRECTIONS

Let us choose a coordinate system with the x-axis parallel to the Sun's rotation axis, the z-axis lying in the solar ecliptic plane and belonging to the plane defined by $\boldsymbol{V}_\infty$ and $0x$ (here we disregard a tilt of the rotation axis with respect to the ecliptic plane), and the y-axis completing a right-handed coordinate system. In this system, the current V1 and V2 heliocentric directions will have spherical coordinates $\theta \approx 35^\circ$, $\phi \approx 2^\circ$ and $\theta \approx 44^\circ$, $\phi \approx 223^\circ$, respectively. Here θ and ϕ are conventional angles of a spherical coordinate system based on the chosen Cartesian system (the θ-angle is measured off the z-axis). Using the results of Lallement et al. (2005) it is easy to calculate that $\boldsymbol{v}_{\rm He}$ and $\boldsymbol{v}_{\rm H}$ within 10 AU are arriving from the directions specified by $\theta \approx 5^\circ$, $\phi = 0$ (by construction of the coordinate system) and $\theta \approx 9^\circ$, $\phi \approx 15^\circ$, respectively. The mutual orientation of the axes of our coordinate system, V1 and V2 trajectories, $\boldsymbol{v}_{\rm He}$, and $\boldsymbol{v}_{\rm H}$ are shown in Figure 1. The angle between the V1 (V2) direction and the direction antiparallel to $\boldsymbol{V}_\infty = \boldsymbol{V}_{\rm He\infty}$ is equal to 30° (48°). That is, the TS distance to the Sun would be considerably smaller in the V2 direction than in the V1 direction, were $\boldsymbol{V}_\infty$ parallel to $\boldsymbol{B}_\infty$. By changing the angle between these two vectors we can try to reverse the asymmetry. Asymmetries of this kind were first predicted by Fahr et al. (1988) on the basis of the Newtonian approximation for compressed flows in the inner and outer heliosheaths. Their existence was later confirmed by numerical simulations in the absence (Pogorelov & Matsuda 1998; Ratkiewicz et al. 1998) and in the presence of the IMF (Pogorelov et al. 2004; Opher et al. 2006). It is clear that a north-south asymmetry of the termination shock can exist regardless of the IMF effects, although bending of the heliospheric current sheet (HCS) behind the termination shock, discovered numerically by Pogorelov et al. (2004), can slightly change this asymmetry. The difference in the TS asymmetry with the IMF and without it can always be compensated by a small ISMF increase. It is also worth noting that when the solar magnetic axis is only slightly tilted with respect to its rotation axis the solution is qualitatively similar to that with zero angle between them (Pogorelov 2006). On the other hand, Pogorelov (2006) has shown that greater tilts ($\alpha_{\rm tilt} \sim 45^\circ$) will effectively smear the effects of the HCS bending.

Using an MHD approximation, disregarding charge exchange processes, and assuming that the B-V plane coincides with the HDP, Opher et al. (2006) found a large difference in the TS standoff distances in the V1 and V2 directions. As shown by Pogorelov et al. (2006) in the presence of magnetic fields and by Pauls & Zank (1997) in their absence, the heliopause becomes considerably less asymmetric with respect to the ecliptic plane when charge exchange is taken into account; that is, charge exchange not only affects the geometrical scale of the heliospheric interface but also tends to symmetrize it. From here on, except in § 4, which deals with the radio emission, we use a two-fluid model, in which only primary (originating in the LISM) hydrogen atoms are taken into account. The effect of symmetrization is illustrated in Figure 2, which shows the plasma temperature distributions for the same SW and LISM parameters, except that in Figure 2*a* charge exchange between neutral hydrogen (H) and plasma is disregarded together with the IMF. Here $\boldsymbol{B}_\infty$ lies in the meridional plane and forms an angle of 45° to the ecliptic plane. It is also assumed that the angle β between $\boldsymbol{V}_\infty$ and the ecliptic plane is zero. The LISM plasma velocity, temperature, and density are $V_\infty = 26.4$ km s^{-1}, $T_\infty = 6527$ K, and $n_\infty = 0.06$ cm^{-3} (LISM parameter set 1), respectively. It is assumed that the SW parameters at 1 AU are the following: $V_{\rm E} = 450$ km s^{-1}, $T_{\rm E} = 51{,}100$ K,

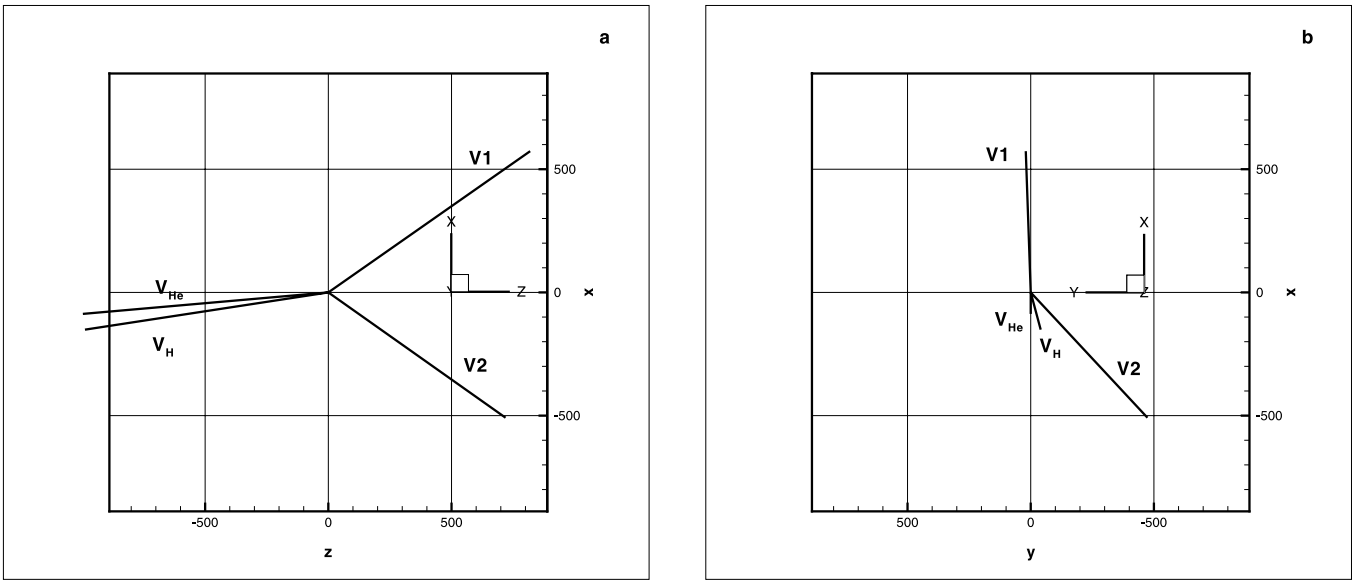

FIG. 1.—Mutual orientation of the *x*-, *y*-, and *z*-axes of our coordinate system, V1 and V2 trajectories, and the neutral He and H velocity directions as measured in the *SOHO* SWAN experiment: (*a*) side view; (*b*) front view.

and $n_E = 7.4$ cm^{-3}. The density of neutral hydrogen is $n_{H\infty} = 0.15$ cm^{-3}. The analysis of the numerical results shows that the TS is closer to the Sun in the V2 direction than in the V1 direction by ~10 AU in the ideal MHD case and by ~2 AU in the MHD-neutral case.

One might expect that asymmetries of the order of those obtained in the purely MHD description could be obtained in the presence of neutrals for a stronger ISMF. However, this suggestion requires some verification. On the one hand, a very strong ISMF perpendicular to the LISM velocity vector can push the TS to unacceptably close distances to the Sun (recall that V1 crossed the TS at about 94 AU). On the other hand, not all ISMF orientations are favorable for the desired asymmetry. If we are considering a TS asymmetry in the *Voyager* directions, then we should recall that $\boldsymbol{V}_\infty$ is not parallel to the *z*-axis. The He velocity vector is known to be tilted at $\beta \sim 5.2^\circ$ to the ecliptic plane (Möbius et al. 2004), while the velocity of the interstellar cloud has a tilt of about 7.8°, according to *Hubble Space Telescope* measurements (Lallement 1996). We can also introduce two angles that specify the ISMF direction $\boldsymbol{B}_\infty$: an angle α_v that $\boldsymbol{B}_\infty$ forms with the velocity vector $\boldsymbol{V}_\infty$, and an angle α_x that it forms with the *x*-axis (the normal to the ecliptic plane). Figures 3*a*–3*c* show the plasma temperature profiles in the V1 (*solid lines*) and V2 (*dashed lines*) directions obtained for different orientations of $\boldsymbol{B}_\infty$ in the HDP ($B_\infty = 3$ μG) for LISM parameter set 1 and the density of neutral hydrogen $n_{H\infty} = 0.15$ cm^{-3}. In contrast to the results of Opher et al. (2006) neither ISMF orientation gives the inferred (Stone et al. 2005) asymmetry of the TS (3, 5, and less than 1 AU, respectively, for Figs. 3*a*, 3*b*, and 3*c*). Furthermore, the change in the $\boldsymbol{B}_\infty$-direction to the opposite of that in Figure 3*b* results in a substantial decrease of the V1-V2 asymmetry (Fig. 3*c*). This means that the HCS behavior and/or numerical merging of the IMF and

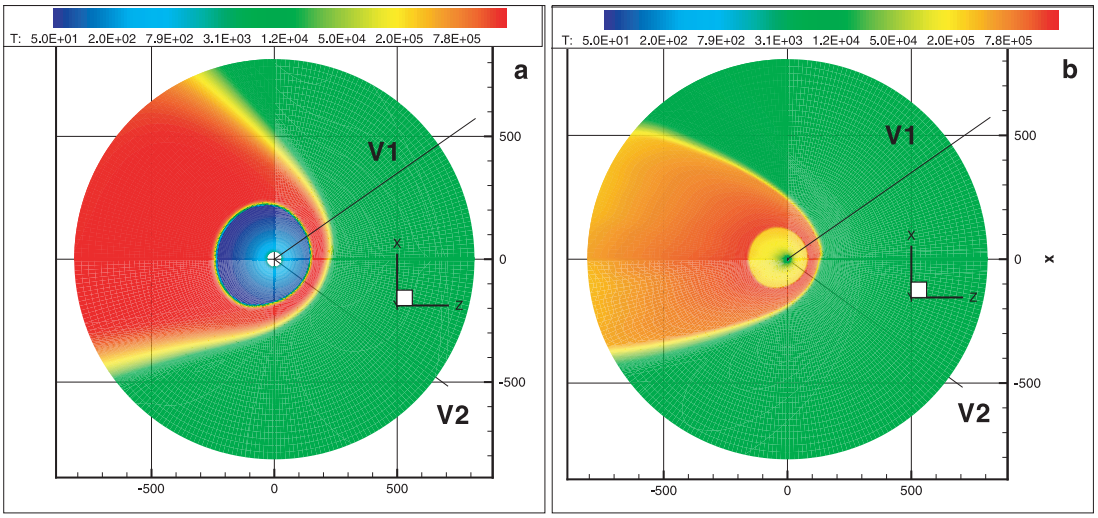

FIG. 2.—Plasma temperature distributions in the meridional plane for $\boldsymbol{B}_\infty$ lying in this plane with a tilt of 45° to the ecliptic plane, $\beta = 0$, and $B_\infty = 2.5$ μG. (*a*) Ideal MHD calculation without an IMF; (*b*) plasma-neutral (two-fluid) model with $n_{H\infty} = 0.15$ cm^{-3} and with an IMF. The straight lines in the northern and southern hemispheres correspond to the V1 and V2 trajectories, respectively. The TS asymmetry is considerably smaller in the case of (*b*) due to the symmetrizing effect of charge exchange.

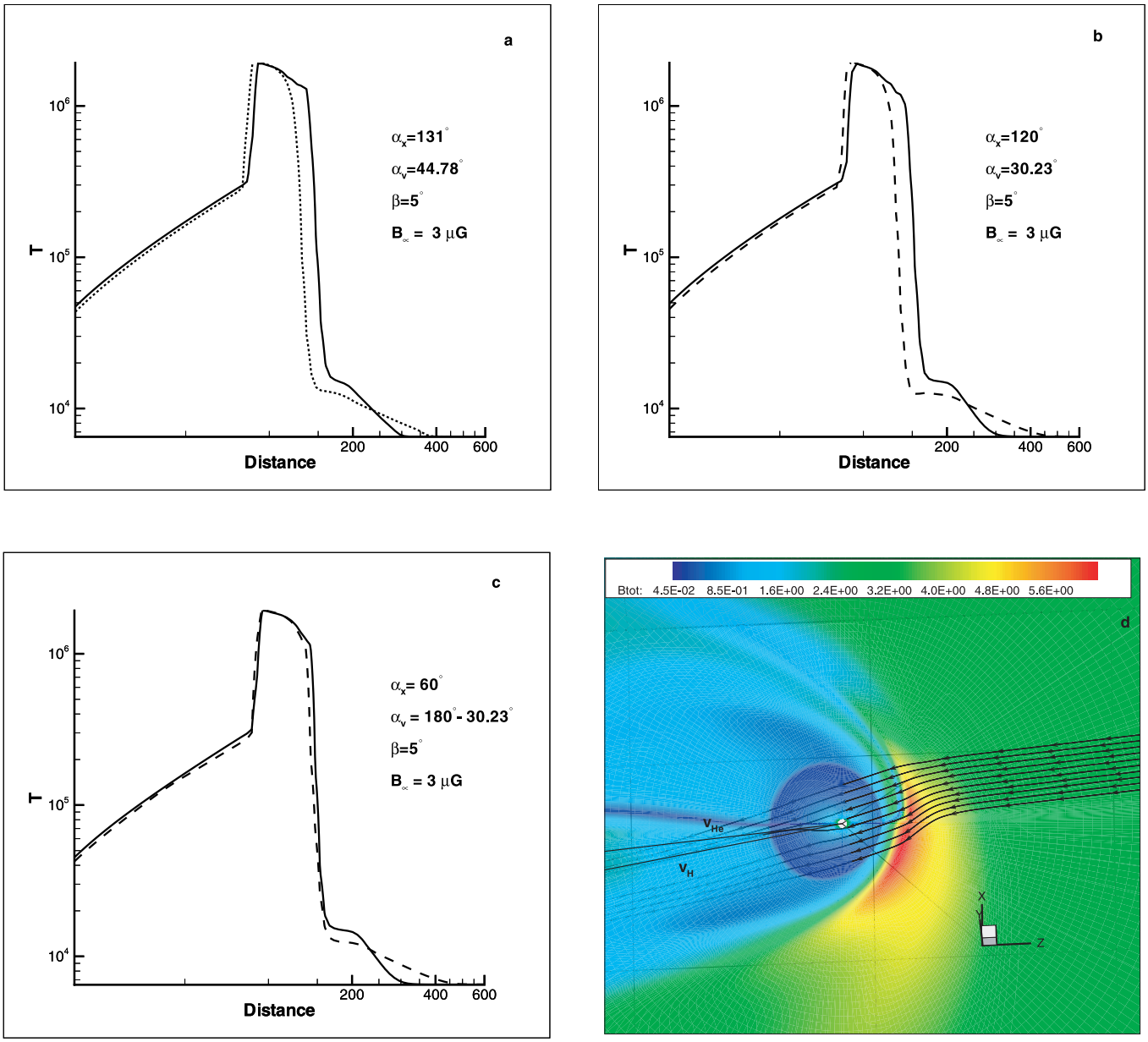

FIG. 3.—(*a*)–(*c*) Plasma temperature distributions along the V1 (*solid lines*) and V2 (*dashed lines*) trajectories for different orientations of $\boldsymbol{B}_\infty$ with respect to the ecliptic plane and $\boldsymbol{V}_\infty$. (*d*) Magnetic field magnitude distribution in the HDP and the streamlines of neutral hydrogen of interstellar origin starting in the HDP in the interval perpendicular to the initial direction of the interstellar hydrogen flow for the parameters corresponding to Fig. 3*b*.

the ISMF lines are important for the numerically obtained asymmetry. The solution without the IMF (not shown) shows a V1-V2 asymmetry of ~3 AU. The HCS bends into the northern hemisphere for the parameters of Figure 3*c*. This is seen in Figure 3*d*, which shows the distribution of the magnetic field magnitude in the *B-V* plane. Besides determining the HDP, another important result of the *SOHO* SWAN experiment (Lallement et al. 2005) is the value of the H-He deflection angle, which by itself restricts a possible asymmetry of the heliosphere. In Figure 3*d*, we show several streamlines of the LISM-borne neutral hydrogen starting in the HDP within the segment of a straight line perpendicular to the direction of neutral helium. In agreement with Pogorelov & Zank (2006) these lines cross the *B-V* plane and disappear behind it. (The heliosphere has no symmetry plane!) As a result, the *B-V* plane does not coincide with the calculated HDP. On the other hand, the angle of the neutral H velocity projection on the *B-V* plane and the neutral He velocity becomes larger than 4°. This means that in our attempt to make the TS asymmetric we increased the H-He deflection above the measured value.

Clearly, there can be other $\boldsymbol{B}_\infty$-directions which result in a TS standoff distance smaller in the V2 than in the V1 direction. For example, this vector can lie in the meridional plane, directed into the southern hemisphere, or in the ecliptic plane, directed at 45° to $\boldsymbol{V}_\infty$ from the west to the east ($B_{y\infty} < 0$). In principle, the latter orientation seems to be very efficient in pushing the TS closer to V2: ~4 and ~7 AU asymmetry for $B_\infty = 2.5$ and 3.5 μG, respectively, and $V_\infty = 25$ km s^{-1}, $T_\infty = 5679$ K, $n_\infty = 0.07$ cm^{-3} (LISM parameter set 2), and $n_{\mathrm{H}\infty} = 0.1$ cm^{-3}. However, this ISMF orientation does not conform with the observed HDP and pushes the TS to unacceptably close distances to the Sun.

It is possible to increase the V1-V2 asymmetry by increasing B_∞ to 4 μG, while decreasing α_v to avoid increasing the magnetic pressure and thus pushing the TS closer to the Sun. We choose $\alpha_v = 15°$, $\alpha_x = 105°$, and $\beta = 0$ for the solution shown

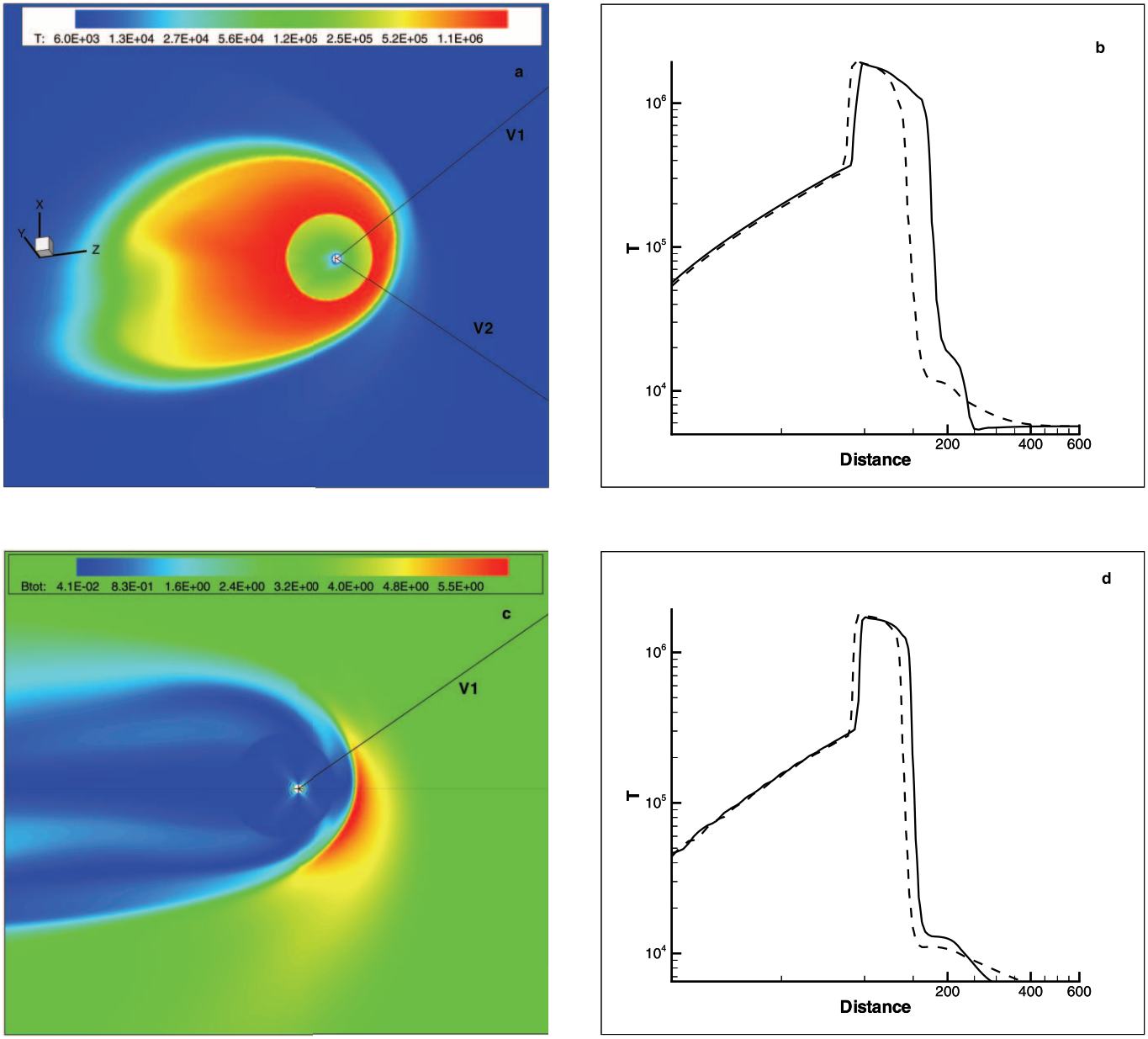

FIG. 4.—(*a*) Plasma temperature distribution in the V1-V2 plane for $B_\infty = 4$ μG, $\alpha_v = 15^\circ$, $\alpha_x = 105^\circ$, $\beta = 0$, and $n_{H\infty} = 0.2$ cm^{-3}. (*b*) Plasma temperature profiles along the V1 (*solid lines*) and V2 (*dashed lines*) directions for the parameters of (*a*). (*c*) Magnetic field magnitude distribution in the meridional plane for the parameters of Fig. 3*b* with the Sun's magnetic axis tilted 45° to its rotation axis. (*d*) Plasma temperature profiles along the V1 (*solid lines*) and V2 (*dashed lines*) direction for the parameters of (*c*).

in Figures 4*a* and 4*b*. We also assume LISM parameter set 2 and $n_{H\infty} = 0.2$ cm^{-3}. The plasma temperature distribution in the V1-V2 plane is shown in Figure 4*a*. The TS distance to the Sun is about 93 and 88 AU in the V1 and V2 directions, respectively. This is seen in Figure 4*b*, which shows the plasma temperature profiles in the V1 and V2 directions. Note that an ISMF of the strength chosen in the previous example was considered to be unlikely by Gloeckler et al. (1997) because of its ability to push the TS very close to the Sun. This is not necessarily so, provided that the angle α_v is small. As shown by Florinski et al. (2004) and Pogorelov et al. (2006) even stronger magnetic fields can be acceptable from this viewpoint. A bow shock may still exist in such cases, but it becomes a slow-mode shock. The presence of neutral hydrogen prevents the HP from moving upstream to infinity, in contrast with the ideal MHD solution of Parker (1961).

Since the Sun's magnetic axis never coincides with its rotation axis, the HCS is not planar in the supersonic solar wind. Its profile is wavy, resembling a ballerina skirt (Jokipii & Thomas 1981). The derivation of the HCS shape based on geometrical considerations is given in the Appendix.

In Figures 4*c* and 4*d* we show the plasma temperature distribution in the meridional plane and their profiles in the V1 and V2 directions for the LISM and SW parameters of Figure 3, but now assuming that the angle between those axes is 45°. The HP surface becomes remarkably smooth in this case, in contrast to the cases with the HCS bent into one of the hemispheres. Because of the ISMF tilt to the LISM velocity vector, magnetic pressure distribution remains asymmetric and the temperature profiles reveal an asymmetry of about 5 AU; that is, the asymmetry is very close to that for the case shown in Figure 3*b*.

3. EAST-WEST ASYMMETRY OF THE TERMINATION SHOCK

If the ISMF has a component parallel to the ecliptic plane directed from the western hemisphere to the eastern hemisphere at an acute angle to $\boldsymbol{V}_\infty$, we can expect an east-west asymmetry of the TS, which would be consistent with the streaming anisotropy of energetic charged particles observed by V1 before it crossed the TS (Krimigis et al. 2003; McDonald et al. 2003). Note that such a component exists if $\boldsymbol{B}_\infty$ belongs to the HDP as observed in the *SOHO* SWAN experiment, as it was in the solutions shown in Figure 3. A calculation showing this has recently been made by Opher et al. (2006) using an ideal MHD model. The effect observed is related to the possibility that certain IMF lines cross the TS, penetrate into the inner heliosheath, and later return into the supersonic SW region, thus connecting a spacecraft there with the compressed plasma in the heliosheath and allowing it to see accelerated proton/ions streaming along magnetic field lines. The IMF lines can cross the TS multiple times because it is shaped more bluntly than the nearly circular magnetic field lines in the upwind region (Jokipii et al. 2004; Pogorelov et al. 2004, 2006; Opher et al. 2006). This phenomenon has recently been used by McComas & Schwadron (2006) and Li & Zank (2006) to suggest an interesting twist to the diffusive acceleration of particles to ACR energies. They suggest that charged particles are injected and accelerated at the TS flanks (where the injection energy threshold is smaller because the shock is more oblique) and are then transported in the heliosheath along an IMF line toward the TS nose where they are observed by V1. A line that crossed the TS at its flank will reach V1 in the inner heliosheath at some distance from the TS. Weak expansion of the inner heliosheath flow ensures that an energized particle will not lose acquired energy while propagating from the energization site to V1. For V1, this will look like the source of ACRs is upstream. McComas & Schwadron (2006) considered only an IMF line lying in the ecliptic plane and used an axially symmetric plasma distribution to estimate the width of the connection region and energies that could be reached. Since each IMF-TS crossing occurs at a higher heliolatitude, we analyze the IMF lines' behavior for three-dimensional cases. Figure 5*a* shows the distribution of plasma temperature in the plane parallel to the ecliptic plane and passing through the point on the V1 trajectory just before it crossed the TS. It also shows the IMF line that starts at this point in both the forward and backward directions. The V1 trajectory is represented by a straight line with direction coinciding with its trajectory. The solution corresponds to LISM parameter set 2 with $n_{\mathrm{H}\infty} = 0.1$ cm^{-3}, $B_\infty = 3.5$ μG, $\alpha_x = 90^\circ$, $\alpha_v = 45^\circ$ ($B_{y\infty} < 0$), and $\beta = 0$.

Of course, we can observe only a projection of the IMF line and the V1 trajectory in Figure 5*a*. Therefore, we cannot see actual TS crossings by the IMF. Instead, they reveal themselves by the increase in the density of the IMF spiral winds. Crossings start in some vicinity of the nose (depending on the asymmetry of the TS). After about 10–11 crossings of either the eastern or western flank of the TS, the spiral leaves the supersonic solar wind and further remains completely in the compressed heliosheath, as compared with the nearly 40 crossings in the analysis of McComas & Schwadron (2006). Crossings are also seen from the distribution of the B_y-component of the IMF along the chosen magnetic field line as a function of the angle $\varphi = -\arctan(y/z)$ (see Fig. 5*b*). While in the supersonic SW, B_y simply changes its sign with the coordinate z, the absolute value decreasing approximately inversely proportional to the distance R from the Sun. The maxima and the minima of the distribution correspond in this case to crossings of the meridional plane in the positive and negative y-directions, respectively. The increase in the local maximum of B_y corresponds to the first penetration of the IMF into the heliosheath. The first increase in the minima indicates that the IMF started crossing the TS in the tail ($z < 0$). The width of the connection region at the heliosheath nose depends on the number of crossings and on the plasma compression in the heliosheath. Figure 5*a* shows that the width of the region swept out by the chosen IMF line is ~10 AU. If B_∞ is smaller, its width increases to about 13 AU for an ISMF strength of 2.5 μG and to about 15 AU for $B_\infty = 1.5$ μG. These distances are smaller than those in the two-dimensional estimates of McComas & Schwadron (2006).

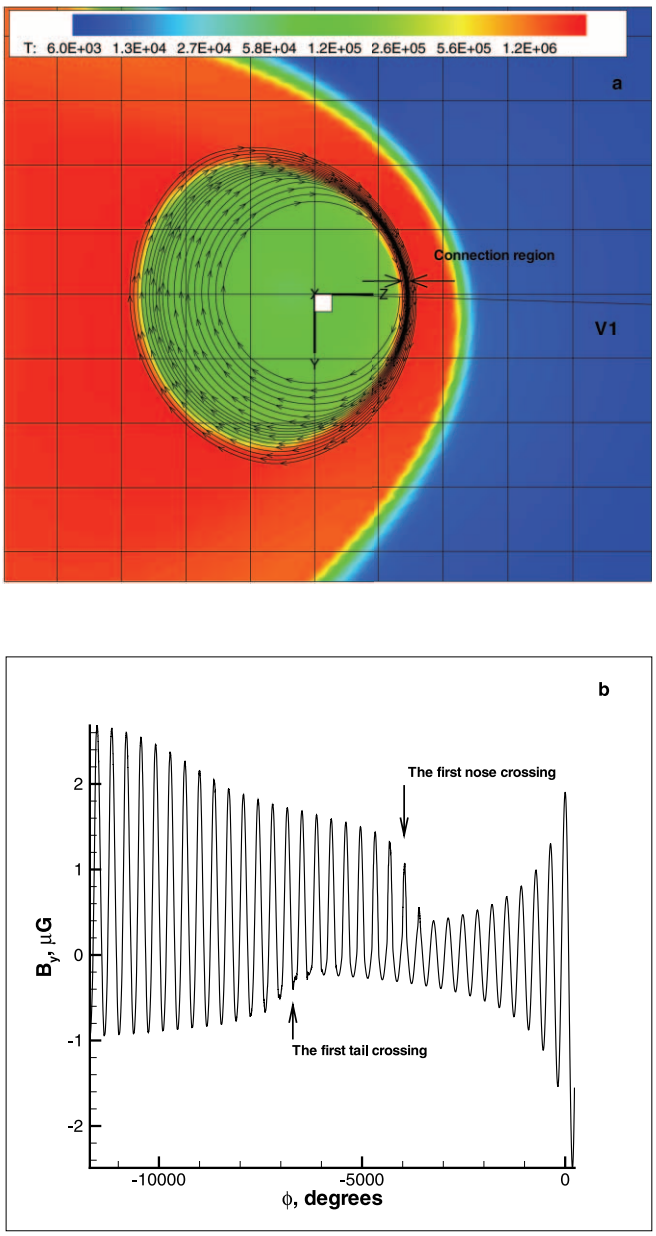

FIG. 5.—(*a*) Plasma temperature distribution in the plane parallel to the ecliptic plane and passing through the V1 location before it crossed the TS, shown together with the IMF line passing through the same point. Note that this line crosses the TS multiple times at gradually increasing heliolatitude. The rectangular grid shown is 50 × 50 AU. (*b*) Distribution of B_y along the IMF line shown above as a function of the polar angle ϕ. The results are obtained for LISM parameter set 2, $B_\infty = 3.5$ μG, $\alpha_x = 90^\circ$, $\alpha_v = 45^\circ$, $\beta = 0$, and $n_{\mathrm{H}\infty} = 0.1$ cm^{-3}. The density of the spiral winds increases as it penetrates into the heliosheath.

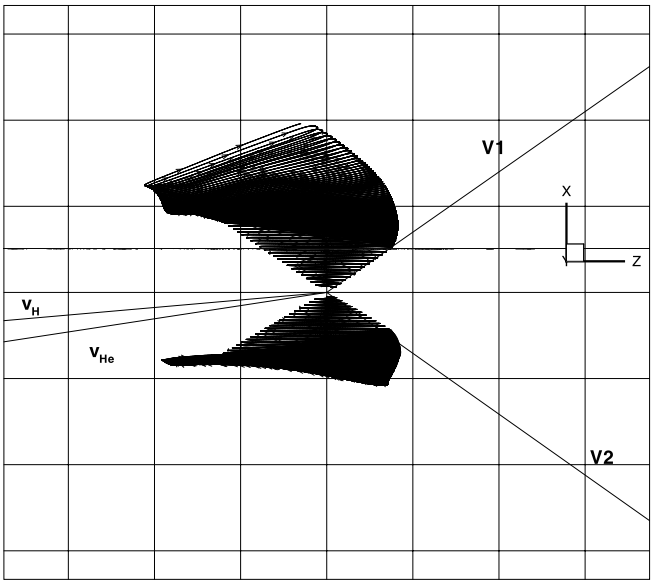

FIG. 6.—Two IMF lines for the simulation with $\boldsymbol{B}_\infty$ belonging to HDP and forming an angle of 30° with $\boldsymbol{V}_\infty$. That in the northern hemisphere crosses the V1 trajectory at about 1 AU before it crosses the termination shock. Note that it bends northward and no longer spirals around the V1 trajectory. The southern-hemisphere IMF line passes through the current V2 location of about 82 AU, that is, 12 AU closer to the Sun than the TS standoff distance at the moment of its crossing by V1. All distances are scaled to the known distance of 94 AU, at which V1 crossed the TS.

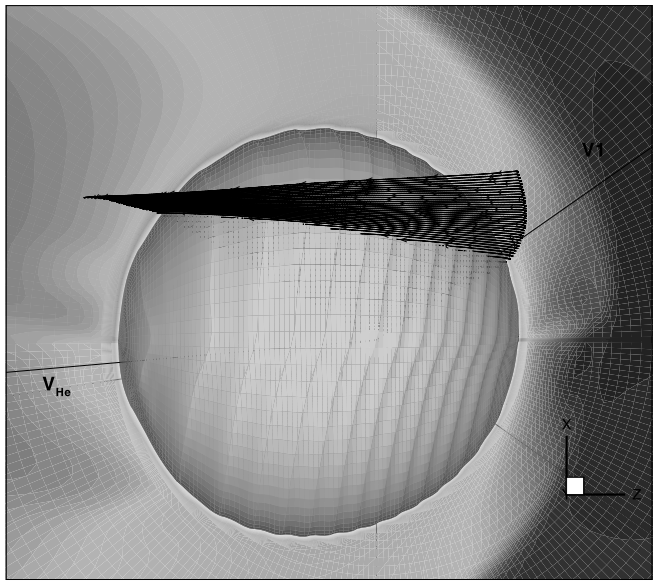

FIG. 7.—TS surface crossed by the last IMF line that crosses the V1 trajectory at least once before it entirely penetrates into the heliosheath. This line determines the V1 connection to the TS.

It should be recognized, however, that V1 moves at an angle to the ecliptic plane and will not cross the same magnetic field line along its trajectory. Figure 6 indicates that V1 will permanently leave the region swept by the chosen IMF line after it crosses the TS. This happens because the IMF line is swept up northward by the SW beyond the shock. The solution shown here corresponds to the set of parameters of Figure 3*b*. That is, $\boldsymbol{B}_\infty$ is in the HDP at 120° to the x-axis ($B_{y\infty} < 0$), and $B_\infty = 3$ μG. Figure 6 shows magnetic field lines passing through V1 right ahead of the TS and through V2 at 82 AU from the Sun, that is, at its location on 2007 February 20. Clearly, such locations of these spacecraft are not simultaneous. The real length of the V1 trajectory covered in the inner heliosheath by different IMF lines directly connected to the TS can be estimated if we analyze the behavior of the lines that start on the V1 trajectory beyond the TS. Figure 7 shows the last of the outermost lines. The others, which cross the V1 trajectory beyond the point corresponding to this line, will not return into the supersonic SW. Note that the width of the connection region along the V1 trajectory is only about 15 AU. This means that V1 will be able to see ACR spectra unrolling according to the scenario suggested by McComas & Schwadron (2006) for ~3.6 yr after it crossed the TS. This does not take into account, of course, the TS motion, which will reduce the connection region for the TS moving toward the Sun and increase it otherwise.

Figures 8*a* and 8*b* show the IMF lines shown in Figure 6 from the top and from the bottom together with the plasma temperature distributions in the planes parallel to the ecliptic plane and passing through the respective spacecraft locations. As seen in these figures, V1 is directly connected to the heliosheath by the corresponding IMF line. The IMF lines crossing the V1 trajectory at distances less than 3 AU from the TS still remain directly connected to the shock. For the set of parameters of Figure 8, V2 becomes directly connected to the TS also at a distance of only about 3 AU from the shock. Before this, V2 is connected to the TS only indirectly, in the direction opposite the IMF winding along a very long arc (more than one full rotation of the IMF spiral). This is not favorable for the particle propagation toward V2 from this direction. The difference between the connections in the northern and southern hemispheres is that the magnetic flux tube connects the segment of the V1 trajectory to the TS in both directions, whereas V2 is connected only in one direction, opposite the direction of the IMF lines forming the tube. The beams of energetic particles streaming along the longer arc of the IMF line experience pitch-angle scattering. The cross-sectional area of the flux tube itself also increases along the field line due to meandering of the field lines. Both of these effects are expected to result in a significant decrease in the intensity of energetic particles reaching the spacecraft along the longer arc.

To estimate a typical minimum energy that a particle must possess in order to propagate upstream from the TS, we observe that a field line that touches the TS at the nose is separated from the shock by about three turns of the spiral at a longitude of 90°. Upstream-traveling particles must be faster than the velocity of the magnetic field line intersection point along the shock surface, i.e., the de Hoffmann–Teller speed, $V_{\rm dHT}$. Since each winding takes $\tau = 26$ days, $V_{\rm dHT} \sim \pi R_{\rm TS}/6\tau \simeq 3.1 \times 10^3$ km s^{-1} (where $R_{\rm TS}$ is the heliocentric distance to the TS), corresponding to a proton energy of about 50 keV. Note that even in the absence of scattering, it would take approximately 1 yr for such a particle to travel one full circle around the Sun along the field line. Higher energy protons, because of their higher velocities (1.4×10^4 km s^{-1} for energies of 1 MeV), can travel a full 360° along the field line in about 2 months. However, this estimate does not take into account the motion of IMF lines. They are convected outward with the SW at a speed of about 400 km s^{-1} (near the TS), covering a radial distance of 6 AU in one solar rotation time τ. This is the distance between the winds of the IMF. The trajectory of V2 becomes directly connected to the TS when the spacecraft is about 3 AU inside the shock. Prior to that, energetic particles can only reach the spacecraft along a long arc of about 390° (one full rotation around the Sun plus an additional ~30° in longitude separating V2 from the nose region, which is assumed to be the source of the particles). IMF lines that cross the V2 trajectory at distances ≥9 AU from the shock make two or more full rotations before

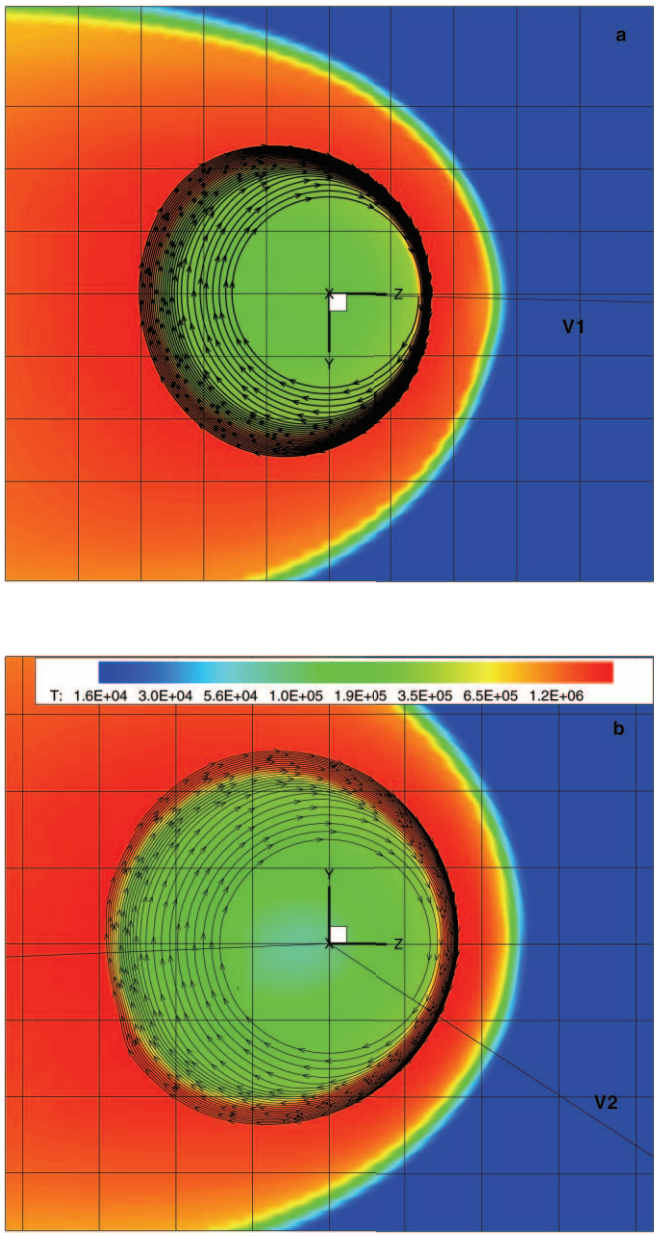

FIG. 8.—(*a*) Plasma temperature distribution in the plane parallel to the ecliptic plane and passing through the V1 location before it crossed the TS, shown together with the IMF line passing through the same point for the parameters of Fig. 3*b*. An IMF line is also shown that starts at the same point. V1 is connected to the heliosheath. (*b*) Plasma temperature distribution in the plane parallel to ecliptic plane and passing through the point on the V2 trajectory at a distance of 82 AU to the Sun (for the parameters of Fig. 3*b*). An IMF line is also shown that starts at the same point. V2 is connected to the heliosheath only backward along this line after more than a full rotation of the spiral. All distances are scaled to the known distance of 94 AU, at which V1 crossed the TS. The rectangular grid shown is 50×50 AU.

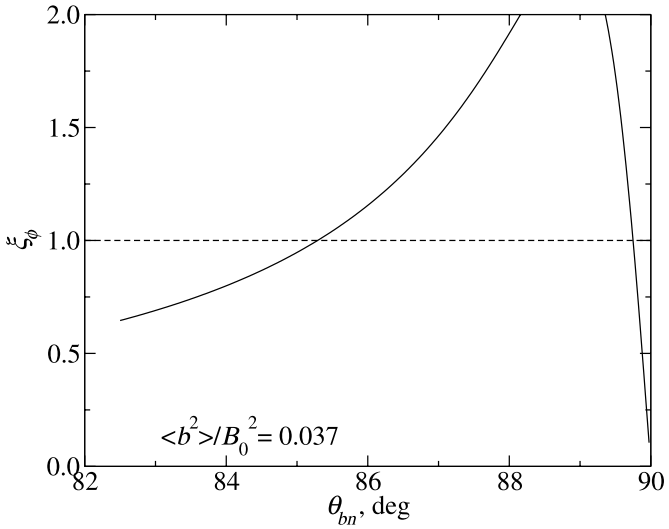

FIG. 9.—Longitudinal streaming anisotropy of 1 MeV protons as a function of the angle θ_{Bn} between the IMF line and the TS normal at the point of their mutual crossing. A dotted line $\xi_\phi = 1$ shows the limits of the applicability of the diffusive theory. It is remarkable that a wide range of possible anisotropies are admissible for nearly perpendicular shocks.

they connect to the TS. This implies that particles must have sufficient energy to complete one full rotation during the interval of time the IMF line propagates the interval along the V2 trajectory starting at 9 AU and ending at 3 AU from the shock, that is, in 26 days. This requires velocities of about 3.6×10^4 km s^{-1}, corresponding to the minimum energy of $\sim$7 MeV for protons. Particles that do not have this minimum energy can only reach V2 along a directly connected field line. The TS distance to the Sun in the V2 direction is equal to $\sim$89 AU in this calculation. This means that V2 started measuring TS particles considerably closer to the Sun (at about 76 vs. 86 AU) than in our stationary SW-LISM interaction model.

As mentioned in § 1, streaming anisotropies of energetic charged particles observed by V1 before crossing the TS may be attributed to the nonalignment of the TS surface with the IMF spirals. It is interesting to estimate quantitatively what streaming anisotropies should be expected for different asymmetries of the TS. Anisotropy with respect to some fixed direction (for instance, the ambient magnetic field vector) is defined as the difference between the particle fluxes in the positive and negative directions along the chosen axis, divided by the total intensity, i.e.,

$$\xi = \frac{f_+ - f_-}{f_+ + f_-}, \tag{1}$$

where $f(\boldsymbol{r}, \boldsymbol{p})$ is the phase space density of energetic particles in the chosen frame (e.g., the SW or the spacecraft frame). An anisotropy so defined can take on values between -1 (all particles moving backward) and +1 (all particles moving forward) with the important intermediate case $\xi = 0$ corresponding to equal numbers of particles moving forward and backward, i.e., to the isotropic distribution.

The largest anisotropy component measured by *Voyager* is in the azimuthal direction. To estimate its magnitude we employ the results of the diffusive theory of particle transport using quasi-linear and NLGC predictions for the parallel and perpendicular mean free paths, respectively. On assuming that the parallel mean free path, $\lambda_\parallel$, is much larger than the perpendicular component, $\lambda_\perp$, the azimuthal anisotropy is easily calculated to be (Zank et al. 2006)

$$\xi_\phi \simeq \frac{3V}{w} \frac{\lambda_\parallel \cos\theta_{Bn} \sin\theta_{Bn}}{\lambda_\perp \sin^2\theta_{Bn} + \lambda_\parallel \cos^2\theta_{Bn}}, \tag{2}$$

where V is the SW radial velocity, w is the particle speed, and θ_{Bn} is the angle between the IMF and the TS normal. The mean free paths are computed using the turbulence transport model as discussed in Zank et al. (2006). The result is shown in Figure 9.

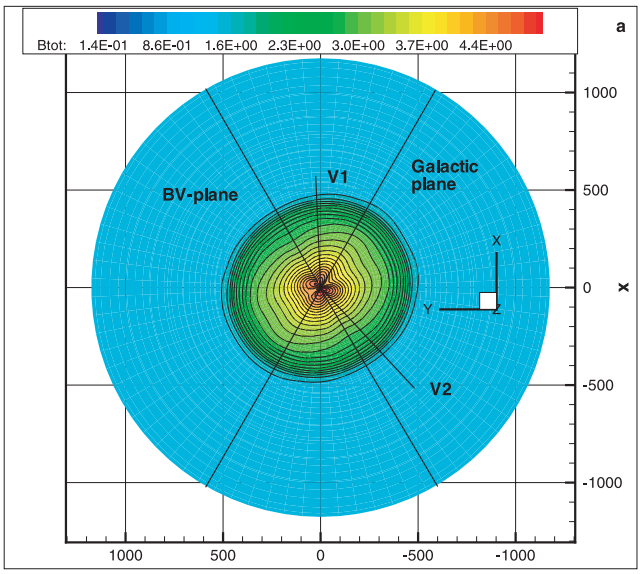

FIG. 10.—Distribution of $|\boldsymbol{B}|$ in the plane perpendicular to $\boldsymbol{V}_\infty$ and intersecting the outer heliosheath. We have used LISM parameter set 1 and assumed $\boldsymbol{B}_\infty$ perpendicular to $\boldsymbol{V}_\infty$ and lying in the plane tilted 60° to the ecliptic plane ($n_{\mathrm{H}\infty} = 0.1$ cm^{-3}, $B_\infty = 1.5$ μG, and $\beta = 0$). The isoline pattern reveals a bandlike structure slightly elongated in the direction perpendicular to the *B-V* plane.

For the solution shown in Figure 5, the angle θ_{Bn} can be estimated to be 84°. This gives $\xi_\phi \approx 0.8$, which is somewhat larger than, but comparable to, the average value of ~0.4 derived from the V1 data (Decker et al. 2006). Anisotropic fluctuations with the value $\xi_\phi \sim 1$ are often measured. Note that the parts of the plot above $\xi_\phi = 1$ should be disregarded, since the assumptions of the diffusive acceleration theory are not satisfied for this region. The figure shows that ξ_ϕ is a rapidly growing function of θ_{Bn}. Thus, the above anisotropy could be observed even without any east-west asymmetry of the TS, since V1 is slightly off the meridional plane (see the discussion in Jokipii et al. 2004). However, the anisotropy of the described type had been observed by V1 for a period of about 3 yr. This indicates that there should be some amount of the east-to-west asymmetry of the TS described in this section, which let V1 measure different IMF lines returning from the heliosheath (Stone et al. 2005). Note also that V1, according to Jokipii (2005) and Richardson et al. (2006), was moving outward with a velocity close to that of the TS during this period.

4. RADIO EMISSION FROM THE OUTER HELIOSHEATH

Although the presence of a GMIR is a necessary condition for the radio emission to be generated in the outer heliosheath, we briefly analyze the influence of the ISMF draping over the HP in determining a preferred plane for the distribution of radio emission sources discovered by Kurth & Gurnett (2003). This has recently been considered by Mitchell et al. (2007) with the application of a simplified (kinematic) distribution of magnetic field in the outer heliosheath. As discussed by Cairns & Zank (2002), one of the conditions for initiating radio emission is a magnetic field strong enough to satisfy the relation $v_r/v_{\mathrm{A}} < 5$. Here v_r is the ring-beam velocity of pickup ions (PUIs) created in the outer heliosheath through charge exchange between the LISM plasma and hot secondary H atoms born in the inner heliosheath, and v_{A} is the Alfvén velocity. We consider two scenarios in this section. (1) We first consider an ISMF perpendicular to the LISM velocity vector ($\boldsymbol{B}_\infty \perp \boldsymbol{V}_\infty$) and lying in the plane passing through the z-axis at 60° to the ecliptic plane in a way indicated in Figure 10, which shows the distribution of $|B|$ in the plane $z = 170$, i.e., intersecting the outer heliosheath. Here we choose LISM parameter set 1, $n_{\mathrm{H}\infty} = 0.1$, and $B_\infty = 1.5$ μG ($B_{x\infty} > 0$). (2) We also consider $\boldsymbol{B}_\infty$ in the HDP for the parameters of Figure 3*b*. In this section, we use a four-fluid model (Pogorelov et al. 2006). For case 1, some signs of a bandlike structure aligned with the direction perpendicular to the *B-V* plane are apparent. However, the aspect ratio is insufficient to describe the observations. This agrees qualitatively with the calculations of Mitchell et al. (2007). In Figure 11, which corresponds to case 2, we show the distribution of $|B|$ in the meridional plane (Fig. 11*a*) and a plane perpendicular to the meridional plane that crosses the region of enhanced *B*

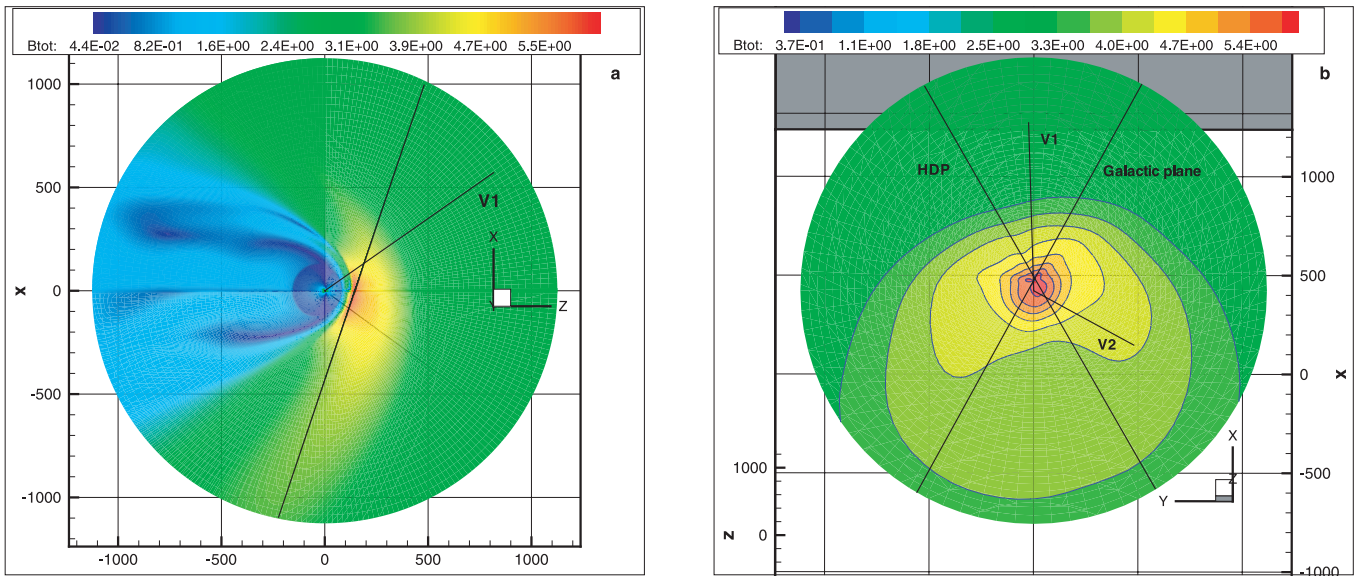

FIG. 11.—(*a*) Magnetic field magnitude distribution in the meridional plane for LISM parameter set 1 and $\boldsymbol{B}_\infty$ in the HDP at 120° to the x-axis ($n_{\mathrm{H}\infty} = 0.15$ cm^{-3}, $B_\infty = 3$ μG, and $\beta = 5°$). Also shown is the V1 trajectory and the plane perpendicular to the meridional plane, which crosses the region of increased magnetic pressure in the outer heliosheath. (*b*) Distribution of $|B|$ in the latter plane showing a bandlike structure that is nearly aligned with the Galactic plane.

TABLE 1
SUMMARY OF THE TS ASYMMETRY IN THE V1 AND V2 DIRECTIONS FOR DIFFERENT SW-LISM INTERACTION PARAMETERS

$\boldsymbol{B}_\infty$ and $\boldsymbol{V}_\infty$	$\alpha_{\rm tilt}$ (deg)	B_∞ (μG)	α_v (deg)	α_x (deg)	β (deg)	$n_{\rm H\infty}$ (cm^{-3})	V1-V2 Asymmetry (AU)
LISM Parameter Set 1							
In the meridional plane.....	No IMF	2.5	45	135	0	0	10
	0	2.5	45	135	0	0.15	2
	0	4	15	105	0	0.2	5
In the HDP.....	0	3	44.78	131	5	0.15	3
	0	3	30.23	120	5	0.15	5
	0	3	149.77	60	5	0.15	<1
	45	3	30.23	120	5	0.15	5
LISM Parameter Set 2							
In the ecliptic plane	0	2.5	45	90	0	0.1	4
	0	3.5	45	90	0	0.1	7

in the outer heliosheath (Fig. 11*b*). The line of intersection of these two planes is shown in Figure 11*a* by an inclined straight line. It is evident from Figure 11*b* that we do not have any distinct band in the magnetic field magnitude distribution. The lines of constant $|B|$ have a raindrop-like shape (see Mitchell et al. 2007) aligned with neither the HDP nor the plane perpendicular to it. One may argue that the drops are elongated in the direction close to the Galactic plane, but it is clear that the drops are shifted southward with respect to the HP nose, which contradicts the observations of Kurth & Gurnett (2003), where most of the radio emission sources are to the north of the nose, being on average parallel to the Galactic plane. Similarly to the case shown in Figure 11*a*, the band is only slightly elongated. This means that the ISMF draping over the HP surface cannot by itself define the location of radio emission sources, and the problem needs to be addressed more generally, including, for example, GMIRs. This will be done elsewhere. It is possible that the Rayleigh-Taylor instability at the HP nose caused by charge exchange between the neutral and plasma components of partially ionized plasma (Zank 1999; Florinski et al. 2005; Kryukov et al. 2006) and the Kelvin-Helmholtz instability of the HP flanks may contribute to the explanation of the observations.

5. DISCUSSION

The role of the ISMF in the deformation and rotation of the HP with respect to a fixed coordinate system is rather well established, having been investigated (see above) both analytically and numerically by a number of authors. With V1 and V2 observations suggesting an asymmetry in heliospheric structure, these models need to confront observational constraints. Most of the LISM parameters, excluding only the ISMF, are reasonably well known. The quantities which are determined best are based on neutral He flow measurements made by different spacecraft missions (these results are summarized by Möbius et al. 2004). Assuming that plasma and neutral particles are in thermal equilibrium in the unperturbed LISM, one can derive the temperature and the bulk velocity vector for these gases. On the basis of *Extreme Ultraviolet Explorer* (*EUVE*) observations, Vallerga (1996) suggested that the number densities for neutral H and ionized hydrogen are within the ranges $0.15 \leq n_{\rm H} \leq 0.34$ and $0.004 \leq n_{\rm H^+} \leq 0.14$, respectively. A neutral H density of $\sim$0.1 cm^{-3} at the TS fits well with the *Ulysses* PUI measurements (Gloeckler et al. 1997; Izmodenov et al. 2003). This value depends on the neutral H filtration in the hydrogen wall ahead of the heliopause, which can be obtained only by numerical experiment. Plasma-neutral calculations based on multifluid and MHD-kinetic simulations (Alexashov & Izmodenov 2005; Heerikhuisen et al. 2006a; Florinski et al. 2003; Pogorelov et al. 2006) restrict $n_{\rm H\infty}$ to the range 0.15–0.2 cm^{-3}. An estimate of the proton number density in the LISM can be inferred from the characteristic size of the heliosphere based on the location of the TS at the moment of its crossing by V1. This density can also be related to the radio emission data (Kurth & Gurnett 2003), resulting in the value of $\sim$0.04 cm^{-3}.

The direction and the magnitude of the ISMF vector are uncertain. Conclusions about the ISMF direction based on the remote observations by Tinbergen (1982) are invalid for the LISM since they were obtained by averaging over a scale of several parsecs. On the other hand, as discussed above, the angle between the *B*-*V* plane and the HDP obtained in the *SOHO* SWAN experiment is hard to determine without numerical modeling.

We show that charge exchange not only considerably decreases the geometrical size of the heliosphere, but also significantly reduces the inferred TS asymmetry, as compared with solutions obtained from ideal MHD calculations (the results are summarized in Table 1). Simple scaling of ideal MHD results to the TS location in the direction of the V1 trajectory is inaccurate. Asymmetries of the TS obtained by Pogorelov & Matsuda (1998) and Opher et al. (2006) are significantly reduced in the presence of neutrals and reasonably small ISMF magnitudes below 2.5 μG. This is seen both from the multifluid calculations of this paper and from the MHD-kinetic modeling of Izmodenov & Alexashov (2006). An increase in the ISMF magnitude, although increasing the asymmetry, also brings the TS to unacceptably close distances (for $\alpha_v > 45^\circ$) to the Sun and increases the deflection between neutral H and He flows measured by Lallement et al. (2005). We show that if the ISMF is the only factor responsible for the TS asymmetry in the V1 and V2 directions, the field should be unexpectedly strong (>4 μG).

Asymmetry can also be introduced by three-dimensional unsteady phenomena. A GMIR considered by Pogorelov & Zank (2005; see also Zank & Müller 2003), on reaching the TS, initially drives it farther from the Sun. This stage lasts not more than 0.5 yr. On reaching its maximum distance from the Sun, the TS location begins to recede, overshooting its initial location. This lasts somewhat less than 1 yr. The relaxation of the TS to its initial location can last for more than 2 yr. The distribution of plasma density in the V1 direction from the moment when the TS reached

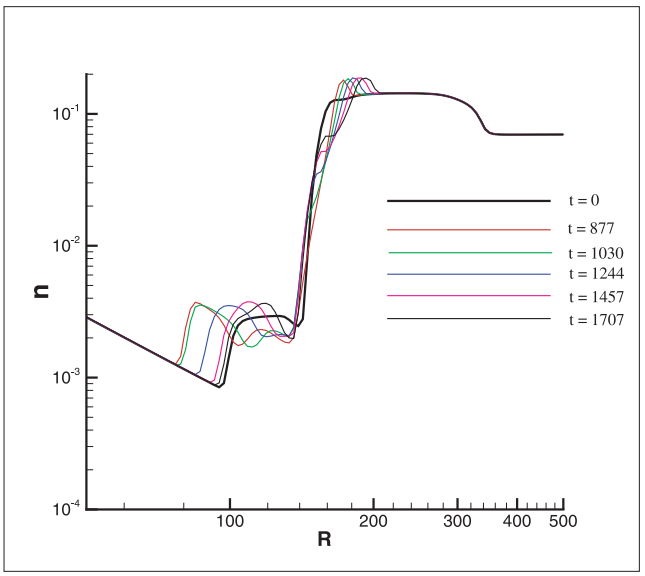

FIG. 12.—Plasma density distribution in the V1 direction for a GMIR propagating through the heliosphere for the SW and LISM parameters from Pogorelov & Zank (2005). The colored curves correspond to the density profiles at different times measured in days from the launch of the perturbation.

its minimum standoff distance until it returned to its initial position is shown in Figure 12. Thus, perturbations caused by a single unsteady event can last for a period that compares to the time V1 observed highly anisotropic energetic particle beams prior to crossing the TS. These arguments are entirely qualitative, and a quantitative analysis will have to be done for specific events, timings, and timescales (see, e.g., Washimi et al. 2006; Richardson et al. 2006, 2007). If a GMIR (or another large perturbation of the SW) is not spherically symmetric, it can introduce a substantial asymmetry in the TS. Moreover, it is likely that even a spherically symmetric perturbation can increase a TS asymmetry introduced by the ISMF. It is interesting to mention that substantial longitudinal streaming anisotropies can be observed by a spacecraft in the immediate vicinity of the TS (ahead of it) even if its trajectory is only slightly off the meridional plane (like that of V1). This is because of the nonalignment of the TS surface with the IMF lines. However, V1 observed energetic particle beams for almost 3 yr, during which time its distance from the Sun increased by $\sim$9 AU. As a result, a certain amount of east-to-west asymmetry of the TS seems to be necessary. Our calculations show that it is impossible to create such asymmetry that would connect V1 at 9 AU from the TS to the heliosheath. This means that V1 and the TS were probably moving at about the same velocity during this period (see also the modeling results of Washimi et al. 2006; Richardson et al. 2007; and the analysis of Jokipii 2005). It is important to distinguish, however, between the TS asymmetry inferred from the observations and that obtained in different numerical models. The asymmetry observed by the *Voyager* spacecraft helps derive important information about the SW and LISM properties. We show here that the answer should be sought in the interplay of the ISMF effects, charge exchange, and transient phenomena in the SW.

We have also considered the observation of medium-energy ACR particles by V1 at the shock and in the inner heliosheath. Their intensity did not increase immediately at the TS, and observations show that it increases as V1 moves farther away from the TS. A possible reason for that, as suggested by McComas & Schwadron (2006), is that from the viewpoint of V1 the source of higher energy particles lies ahead of it. A possible explanation is that V1 is directly connected to the TS flanks by IMF lines. McComas & Schwadron (2006) derived the characteristic maximum energy that particles can reach if they are injected into the shock-acceleration process at different longitudes. Although that scenario is based on two-dimensional heliospheric calculations, and therefore makes estimates in the vicinity of the ecliptic plane, it is still valid at the latitudes of the V1 trajectory. The difference between the two- and three-dimensional cases is essential because each crossing of the TS by an IMF line occurs at progressively increasing latitudes. Since the trajectory of V1 is nearly a straight line aligned with its radius-vector starting at the Sun, it essentially remains on the same IMF-line cone in the supersonic SW region. After crossing the TS, the line spiraling along the surface of this cone turns northward to higher latitudes. This means that all those points on the V1 trajectory in the heliosheath that are connected to IMF lines were initially at latitudes lower than that of the TS. Our analysis shows that the width of the connection region in this case is considerably narrower than the connection near the ecliptic plane. Our model, which is essentially based on steady boundary conditions in the SW, gives a width of the connection region of close to 15 AU.

Finally, consider the possibility of using the 2–3 kHz radio emission data to determine the ISMF properties. The radio emission sources so far appear to be aligned with the Galactic plane. We find that the draping of the ISMF around the heliopause can indeed create a bandlike distribution of the magnetic field pressure in the outer heliosheath. For orientations of the *B*-*V* plane that are reasonably consistent with the HDP orientation, the bands are slightly elongated in the direction the Galactic plane. For the $\alpha_v = 90^\circ$ the bands are nearly aligned with the plane perpendicular to the *B*-*V* plane, but some misalignment is introduced by smaller angles. On the other hand, the maximum of the ISMF pressure is systematically shifted to the south from the ecliptic plane, which does not agree with the observations. In summary, we believe that the asymmetry of the magnetic pressure caused by the ISMF draping around the HP is unlikely to be sufficient for creating the observed asymmetry of the radio-emission sources. To find a convincing answer to this problem, it is important to consider simulation results in close connection with the physical theory explaining the origin of radio emission in the outer heliosphere.

There is no doubt that unsteady SW phenomena together with the ISMF make the heliosphere asymmetric. Asymmetries created by the ISMF can last for a long time, provided that the properties of the LISM are slowly varying. Asymmetries caused by a nonuniform SW have shorter timescales. Here we show the importance of charge exchange for the accurate analysis of such asymmetries. This is not only because neutrals significantly reduce the asymmetry of the heliosphere (the LISM plasma is rather weakly ionized), but also because neutral hydrogen itself serves as a measure of the heliospheric asymmetry; a larger asymmetry results in a larger deflection of neutral H from the neutral He flows.

This work was supported by NASA grants NNG05GD45G, NNG06GD48G, and NNG06GD43G and NSF award ATM-0296114. Calculations were performed on the supercomputers Fujitsu Primepower HPC2500, in the framework of the collaborative agreement with the Solar-Terrestrial Environment Laboratory of Nagoya University, Columbia at NASA Ames Research Center (award SMD-06-0167), and IBM DataStar, on the basis of the Academic Associates Program and award ATM-070011, at the San Diego Supercomputer Center.

APPENDIX

THE SHAPE OF THE HCS

Here we use some simple considerations that allow us to derive the shape of the HCS if the magnetic axis of the Sun, whose magnetic field is assumed to be dipole, is tilted at an angle γ to its rotation axis. Our results generalize the formulae by Jokipii & Thomas (1981) to nonsmall tilt angles. Figure 13 illustrates the geometry of the problem. Here z is the solar rotation axis, which is here assumed to be perpendicular to the ecliptic plane, and z' is the direction of the dipole. The neutral sheet is modeled as a plane inclined to the ecliptic plane by the angle γ (neutral sheet tilt angle). Point C is a footpoint of a magnetic field line on the Sun, or, perhaps, at the Alfvén radius.

In the coordinate system $0x'y'z'$ the curve describing a unit circle lying in the plane of the sheet is given by

$$x'^2 + y'^2 = 1, \qquad z' = 0. \tag{A1}$$

The coordinate transformation to the heliographic system $0xyz$ is

$$x' = x, \qquad y' = y\cos\gamma + z\sin\gamma, \qquad z' = z\cos\gamma - y\sin\gamma. \tag{A2}$$

The equation for the tilted circle in the heliographic coordinate system is then

$$x^2 + (y\cos\gamma + z\sin\gamma)^2 = 1, \qquad z\cos\gamma - y\sin\gamma = 0. \tag{A3}$$

To find the dependence of $\theta(\varphi)$ we note that the coordinates of point C satisfy

$$\tan\varphi = \frac{y}{x}, \qquad \sin\theta = z. \tag{A4}$$

From equation (A3) one obtains

$$\tan^2\varphi = \frac{z^2\cos^2\gamma}{\sin^2\gamma - z^2}, \tag{A5}$$

and finally

$$\theta = \sin^{-1}\left[\frac{\sin\gamma\sin\varphi}{|\cos\varphi|(\cos^2\gamma + \tan^2\varphi)^{1/2}}\right]. \tag{A6}$$

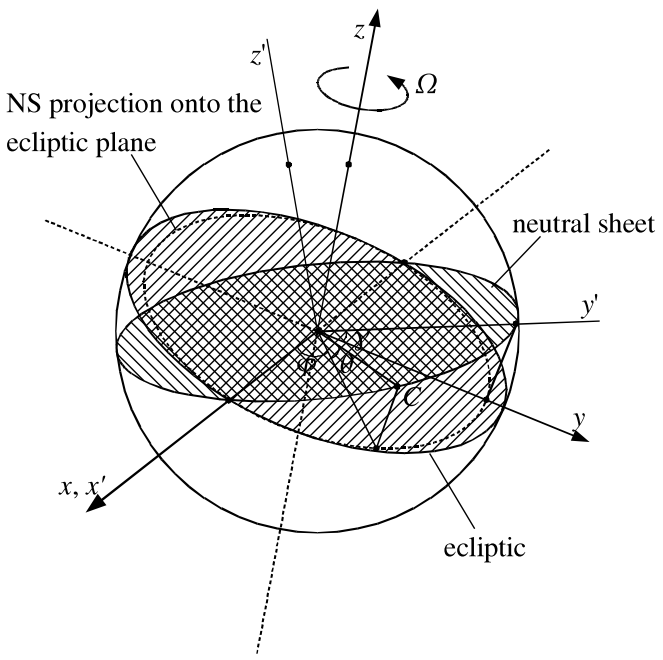

FIG. 13.—HCS (neutral sheet) geometry for the Sun's magnetic dipole axis ($0z'$) tilted to its rotation axis ($0z$) by an angle α.

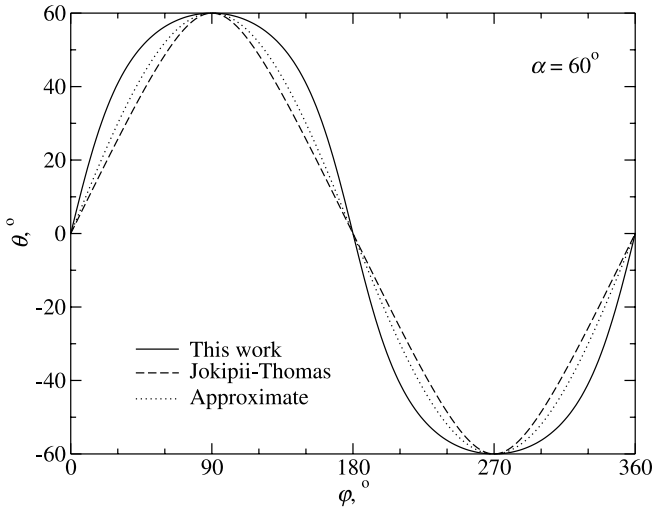

FIG. 14.—HCS (neutral sheet) latitude as a function of the azimuthal angle φ for the angle between the Sun's magnetic and rotation axes equal to 60°. The curve labeled "Jokipii-Thomas" is plotted from eq. (A7), and the curve labeled "approximate" uses eq. (A8).

Note that the result obtained is different from the expression given by Jokipii & Thomas (1981),

$$\theta_{\rm JT} = \sin^{-1}(\sin\gamma \sin\varphi). \tag{A7}$$

From Figure 13 one can see that the latter expression is obtained by taking $\tan\varphi = y'/x$ instead of equation (A4), i.e., if one measures the azimuthal angle in the plane of the HCS instead of the ecliptic plane. When the tilt angle is small both expressions tend to the same limit,

$$\theta \simeq \gamma \sin\varphi, \tag{A8}$$

but they are different when γ is large (see Fig. 14).

To derive the expression giving the shape of the neutral sheet at other heliocentric distances at arbitrary time t one notes that for $R \gg R_\odot$ (the solar radius) the SW expands radially with velocity V dragging the IMF with it, while the field line footpoint C corotates with the Sun at the angular speed Ω. Then a field line at a position (R, φ) and time t is traced back to the point $(0, \varphi_0)$ at $t = 0$ where

$$\varphi_0 = \varphi + \frac{\Omega R}{V} - \Omega t \tag{A9}$$

and the shape of the neutral sheet is given by

$$\theta(r, \varphi, t) = \theta_0(0, \varphi_0, 0), \tag{A10}$$

where θ_0 is given by equation (A6). This gives us the shape known as a "ballerina skirt."

REFERENCES

Alexashov, D., & Izmodenov, V. 2005, A&A, 439, 1171
Cairns, I. H., Mitchell, J. J., Pogorelov, N. V., & Zank, G. P. 2006, in AIP Conf. Proc. 858, Physics of the Inner Heliosheath, ed. J. Heerikhuisen et al. (New York: AIP), 329
Cairns, I. H., & Zank, G. P. 2002, Geophys. Res. Lett., 29, 1143
Decker, R. B., Roelof, E. C., Krimigis, S. M., & Hill, M. E. 2006, in AIP Conf. Proc. 858, Physics of the Inner Heliosheath, ed. J. Heerikhuisen et al. (New York: AIP), 73
Fahr, H. J., Grzedzielski, S., & Ratkiewicz, R. 1988, Ann. Geophys., 6, 337
Florinski, V., Pogorelov, N. V., Zank, G. P., Wood, B. E., & Cox, D. P. 2004, ApJ, 604, 700
Florinski, V., Zank, G. P., & Pogorelov, N. V. 2003, J. Geophys. Res., 108, 1228
———. 2005, J. Geophys. Res., 110, A071104
Frisch, P. C. 2003, ApJ, 593, 868
Gloeckler, G., Fisk, L. A., & Geiss, J. 1997, Nature, 386, 374
Gurnett, D. A., Kurth, W. S., Cairns, I. H., & Mitchell, J. J. 2006, in AIP Conf. Proc. 858, Physics of the Inner Heliosheath, ed. J. Heerikhuisen et al. (New York: AIP), 129
Heerikhuisen, J., Florinski, V., & Zank, G. P. 2006a, J. Geophys. Res., 111, A06110
Heerikhuisen, J., Pogorelov, N., Florinski, V., & Zank, G. 2006b, in AIP Conf. Proc. 858, Physics of the Inner Heliosheath, ed. J. Heerikhuisen et al. (New York: AIP), 263
Heerikhuisen, J., Pogorelov, N., Zank, G., & Florinski, V. 2007, ApJ, 655, L53
Izmodenov, V., Alexashov, D., & Myasnikov, A. 2005, A&A, 437, L35
Izmodenov, V., Malama, Y. G., Gloeckler, G., & Geiss, J. 2003, ApJ, 594, L59
Izmodenov, V. V., & Alexashov, D. B. 2006, in AIP Conf. Proc. 858, Physics of the Inner Heliosheath, ed. J. Heerikhuisen et al. (New York: AIP), 14
Jokipii, J. R. 2005, ApJ, 631, L163
Jokipii, J. R., Giacalone, J., & Kóta, J. 2004, ApJ, 611, L141
Jokipii, J. R., & Thomas, B. 1981, ApJ, 243, 1115
Krimigis, S. M., Decker, R. B., Hill, M. E., Armstrong, T. P., Gloeckler, G., Hamilton, D. C., Lanzerotti, L. J., & Roelof, E. C. 2003, Nature, 426, 45
Kryukov, I. A., Borovikov, S. N., Pogorelov, N. V., & Zank, G. P. 2006, in AIP Conf. Proc. 858, Physics of the Inner Heliosheath, ed. J. Heerikhuisen et al. (New York: AIP), 39
Kurth, W. S., & Gurnett, D. A. 2003, J. Geophys. Res., 108, 8027

Lallement, R. 1996, Space Sci. Rev., 78, 361
Lallement, R., Quémerais, E., Bertaux, J. L., Ferron, S., Koutroumpa, D., & Pellinen, R. 2005, Science, 307, 1447
Li, G., & Zank, G. P. 2006, in AIP Conf. Proc. 858, Physics of the Inner Heliosheath, ed. J. Heerikhuisen et al. (New York: AIP), 183
McComas, D., et al. 2004, in AIP Conf. Proc. 719, Physics of the Outer Heliosphere, ed. V. Florinski, N. V. Pogorelov, & G. P. Zank (New York: AIP), 162
McComas, D. J., & Schwadron, N. A. 2006, Geophys. Res. Lett., 33, L04102
McComas, D. J., et al. 2006, in AIP Conf. Proc. 858, Physics of the Inner Heliosheath, ed. J. Heerikhuisen, et al. (New York: AIP), 241
McDonald, F. B., Stone, E. C., Cummings, A. C., Heikkila, B., Lal, N., & Webber, W. R. 2003, Nature, 426, 48
Mitchell, J. J., Cairns, I. H., Pogorelov, N. V., & Zank, G. P. 2007, J. Geophys. Res., in press
Möbius, E., et al. 2004, A&A, 426, 897
Opher, M., Stone, E. C., & Liewer, P. C. 2006, ApJ, 640, L71
Parker, E. N. 1961, ApJ, 134, 20
Pauls, H. L., & Zank, G. P. 1997, J. Geophys. Res., 102, 19779
Pogorelov, N. V. 2006, in AIP Conf. Proc. 858, Physics of the Inner Heliosheath, ed. J. Heerikhuisen et al. (New York: AIP), 3
Pogorelov, N. V., & Matsuda, T. 1998, J. Geophys. Res., 10, 237
Pogorelov, N. V., & Zank, G. P. 2005, in Proc. Solar Wind 11–*SOHO* 16, Connecting Sun and Heliosphere, ed. B. Fleck, T. H. Zurbuchen, & H. Lacoste (ESA SP-592; Noordwijk: ESA), 35
———. 2006, ApJ, 636, L161
Pogorelov, N. V., Zank, G. P., & Ogino, T. 2004, ApJ, 614, 1007
Pogorelov, N. V., Zank, G. P., & Ogino, T. 2006, ApJ, 644, 1299
Ratkiewicz, R., Barnes, A., Molvik, G. A., Spreiter, J. R., Stahara, S. S., & Vinokur, M. 1998, A&A, 335, 363
Ratkiewicz, R., Barnes, A., & Spreiter, J. R. 2000, J. Geophys. Res., 105, 25021
Ratkiewicz, R., & Ben-Jaffel, L. 2002, J. Geophys. Res. Space Phys., 107, 1007
Richardson, J. D., Liu, Y., & Wang, C. 2007, Adv. Space. Res., in press
Richardson, J. D., Wang, C., & Zhang, M. 2006, in AIP Conf. Proc. 858, Physics of the Inner Heliosheath, ed. J. Heerikhuisen et al. (New York: AIP), 110
Stone, E. C., Cummings, A. C., McDonald, F. B., Heikkila, B., Lal, N., & Webber, W. R. 2005, Science, 309, 2017
Tinbergen, J. 1982, A&A, 105, 53
Vallerga, J. V. 1996, Space Sci. Rev., 78, 277
Washimi, H., Zank, G. P., & Tanaka, T. 2006, in AIP Conf. Proc. 858, Physics of the Inner Heliosheath, ed. J. Heerikhuisen et al. (New York: AIP), 58
Wood, B. E., Izmodenov, V. V., & Pogorelov, N. V. 2006, in AIP Conf. Proc. 858, Physics of the Inner Heliosheath, ed. J. Heerikhuisen et al. (New York: AIP), 335
Wood, B. E., Müller, H.-R., Zank, G. P., Izmodenov, V. V., & Linsky, J. L. 2004, Adv. Space Res., 34, 66
Zank, G. P. 1999, Space Sci. Rev., 89, 413
Zank, G. P., Li, G., Florinski, V., Hu, Q., Lario, D., & Smith, C. W. 2006, J. Geophys. Res., 111, A06108
Zank, G. P., & Müller, H.-R. 2003, J. Geophys. Res. Space Phys., 108, 1240